Applied Catalysis B: Environmental 250 (2019) 10–16

Contents lists available at ScienceDirect

Applied Catalysis B: Environmental

journal homepage: www.elsevier.com/locate/apcatb

Photo-assisted methanol synthesis via CO_2 reduction under ambient pressure over plasmonic Cu/ZnO catalysts

Zhou-jun Wang[a,b,1], Hui Song[b,c,1], Hong Pang[b,c], Yanxiao Ning[j], Thang Duy Dao[b,f,g], Zhuan Wang[h,i], Hailong Chen[h,i], Yuxiang Weng[h,i], Qiang Fu[j], Tadaaki Nagao[b,f,g], Yunming Fang[a,**], Jinhua Ye[b,c,d,e,*]

[a] State Key Laboratory of Chemical Resource Engineering, Beijing Key Laboratory of Energy Environmental Catalysis, Beijing University of Chemical Technology, Beijing, 100029, PR China
[b] International Center for Materials Nanoarchitectonics (WPI-MANA), National Institute for Materials Science (NIMS), 1-1 Namiki, Tsukuba, Ibaraki, 305-0044, Japan
[c] Graduate School of Chemical Sciences and Engineering, Hokkaido University, Sapporo, 060-0814, Japan
[d] TJU-NIMS International Collaboration Laboratory, School of Material Science and Engineering, Tianjin University, Tianjin, 300072, PR China
[e] Collaborative Innovation Center of Chemical Science and Engineering (Tianjin), Tianjin, 300072, PR China
[f] CREST, Japan Science and Technology Agency (JST), 4-1-8 Honcho, Kawaguchi, Saitama, 332-0012, Japan
[g] Department of Condensed Matter Physics, Graduate School of Science, Hokkaido University, Kita-10 Nishi-8 Kita-ku, Sapporo, 060-0810, Japan
[h] Condensed Matter Physics, Institute of Physics, Chinese Academy of Sciences, Beijing, 100190, PR China
[i] School of Physical Sciences, University of Chinese Academy of Sciences, Beijing, 100049, PR China
[j] State Key Laboratory of Catalysis, iChEM, Dalian Institute of Chemical Physics, Chinese Academy of Sciences, Dalian, 116023, PR China

ARTICLE INFO

Keywords:
Photocatalysis
Carbon dioxide
Reduction
Copper
Surface plasmon resonance

ABSTRACT

Methanol synthesis *via* carbon dioxide (CO_2) reduction is challenging and important because this technology can convert CO_2 by solar- or wind-generated hydrogen into liquid fuel. The present work introduces the visible light as an external stimulus and for the first time demonstrates that methanol synthesis over Cu/ZnO catalysts can be effectively promoted by solar energy under atmospheric pressure. Experimental and theoretical studies document that hot electrons were photo-excited by localized surface plasmon resonance (LSPR) on Cu nanoparticles and such photo-excited hot electrons could transfer to ZnO through the metal-support interfaces. The hot electrons on Cu and ZnO synergistically facilitated the activation of reaction intermediates. Consequently, the activation energy was reduced by 40% and the methanol synthesis activity was promoted by 54%. This work provides a new strategy towards synthesis of liquid fuel *via* CO_2 reduction under low pressure and sheds new light on the mechanism of photo-mediated catalysis.

1. Introduction

Carbon dioxide (CO_2) is one of the potent greenhouse gases and an abundant carbon building block [1–5]. Converting CO_2 into high calorific fuels is of great significance because this technology can simultaneously alleviate global warming and energy crisis. A particularly attractive route is to reduce CO_2 into methanol *via* hydrogenation, which can utilize H_2 from renewable sources [6–10]. Methanol is among the top ten commodity chemicals (70 MMT in 2015) with wide applications as a fuel or a chemical feedstock, which plays a prominent role in industry [11–13].

Although methanol has been commercially produced from syngas (H_2/CO) containing CO_2 up to 30% of the total carbon over Cu-ZnO-Al_2O_3 catalysts at 200–300 °C under 5.0–10.0 MPa, low methanol yields are obtained with pure CO_2 as the carbon source [14–16]. Another technical hurdle is the low methanol yields under low pressure, which would impede the decentralized use of solar- or wind-generated H_2 [17,18]. To enhance methanol yields under low pressure, various novel catalysts such as a Ni-Ga catalyst [19], Au nanoparticles activated on a CeO_x/TiO_2 interface [20] and a Ni-In-Al/SiO_2 catalyst [21] were designed. In the meantime, recent work documented that catalytic performance could be markedly improved with the design of

* Corresponding author at: International Center for Materials Nanoarchitectonics (WPI-MANA), National Institute for Materials Science (NIMS), 1-1 Namiki, Tsukuba, Ibaraki, 305-0044, Japan.
** Corresponding author.
E-mail addresses: fangym@mail.buct.edu.cn (Y. Fang), Jinhua.YE@nims.go.jp (J. Ye).
[1] These authors contributed equally to this work.

https://doi.org/10.1016/j.apcatb.2019.03.003
Received 5 December 2018; Received in revised form 7 February 2019; Accepted 1 March 2019
Available online 02 March 2019
0926-3373/

photocatalysis-based materials [22,23]. In this context, an alternative strategy to promote methanol synthesis is to introduce light as an extra stimulus to lower the activation barrier of the traditional, phonon-driven thermal reaction *via* an electron-driven photocatalytic mechanism [24–27]. It has been demonstrated that noble metal (Au, Ag, Cu) nanostructures, which interact with solar energy by an excitation of localized surface plasmon resonance (LSPR), can serve as plasmonic promoters and enhance the catalytic efficiency under light irradiation [28–33]. For example, Hao and co-workers [28] reported highly selective photocatalytic hydrogenation of cinnamaldehyde over plasmonic Au nanoparticles supported on SiC. Linic's group [29] found that on the plasmonic Ag nanostructures, catalytic oxidation reactions could be accomplished at much lower temperature by coupling solar energy with thermal energy. Lyu et al. [30] observed that the activity of CuPt nanoframes in 4-nitrophenol reduction was enhanced to ~1.3 times under visible light irradiation due to LSPR effect on the Cu-rich skeleton. Our group [31,29–33] recently found that under visible light irradiation, Au nanoparticles as a plasmonic promoter in bimetallic dry reforming catalysts could effectively enhance CO_2 activation and improve the catalytic performance. Much surprisingly, no relevant work has been reported on plasmonic Cu nanostructures for methanol synthesis *via* CO_2 reduction.

Herein, a Cu/ZnO catalyst was employed as a model catalyst for methanol synthesis *via* CO_2 reduction because the Cu/ZnO system has emerged as a prototype for the fundamental studies towards the complicated catalysts for methanol synthesis [9,34]. The visible light was introduced as an extra stimulus aiming to enhance the catalytic performance. The mechanisms underlying the visible light promoted methanol synthesis were unravelled by the combination of experimental and theoretical studies.

2. Experimental section

2.1. Materials

$Cu(NO_3)_2{\cdot}3H_2O$ (99.9%), $Zn(NO_3)_2{\cdot}6H_2O$ (99.9%), Na_2CO_3 (99.9%), $Ce(NO_3)_3{\cdot}6H_2O$ (98.0%), and $ZrO(NO_3)_2{\cdot}2H_2O$ (97.0%) were purchased from Wako Pure Chemical Industries, Ltd. TiO_2 (AEROXIDE® TiO_2 P25) was purchased from Evonik-Degussa. All of the chemicals were used as received.

2.2. Catalyst preparation

The Cu/ZnO catalyst with Cu/Zn molar ratio of 1/2 was prepared with a co-precipitation method [35,36]. An aqueous solution containing 0.05 M of $Cu(NO_3)_2{\cdot}3H_2O$ and 0.1 M of $Zn(NO_3)_2{\cdot}6H_2O$ as the metal precursor, and an aqueous solution containing 0.15 M of Na_2CO_3 as the precipitant were added simultaneously into 200 ml of deionized water at a constant pH of 7.0 under vigorous stirring at 70 °C. The co-precipitation step was finished after 100 ml of metal precursor solution was added. The obtained slurry was aged for 2 h at 70 °C. After being cooled to room temperature, the precipitate was filtered and washed thoroughly with deionized water. The collected sample was then dried at 110 °C overnight and calcined at 350 °C for 4 h.

Besides, two series of reference catalysts were prepared with similar procedures as described above. The first one are Cu/ZnO catalysts with other Cu/Zn molar ratios (1/4, 1/1 and 2/1), which were prepared with Cu/Zn molar ratios in the metal precursor solution being varied accordingly. The second one are Cu catalysts supported on other oxides (CeO_2, ZrO_2 and TiO_2). Cu/CeO_2 and Cu/ZrO_2 catalysts were prepared using $Ce(NO_3)_3{\cdot}6H_2O$ and $ZrO(NO_3)_2{\cdot}2H_2O$ as the metal precursor instead. Due to the quick hydrolysis of titanium precursor, the Cu/TiO_2 catalyst was prepared by the incipient wetness impregnation method using P25 as the support.

2.3. Catalyst characterization

N_2 sorption was carried out on a BEL Sorp-II mini instrument (BEL Japan, Inc.) at −196 °C. The specific surface area was determined by the Brumauer-Emmett-Teller (BET) method. X-ray diffraction (XRD) patterns were recorded on an X'Pert PRO diffractometer with a Cu Kα radiation. The phase identification was made by indexing the Joint Committee on Powder Diffraction Standards (JCPDS) database. High resolution-transmission electron microscopy (HR-TEM) images were collected on a JEM-2100 F microscope (JEOL Ltd., Japan) at a working voltage of 200 kV. X-ray photoelectron spectroscopy (XPS) and auger electron spectroscopy (AES) spectra were acquired in a SPECS multi-technique surface analysis system that was equipped with an Al Kα X-ray source (1486.7 eV) and a PHOIBOS 100 hemispherical energy analyzer. To avoid the facile oxidation of metallic Cu under ambient conditions, the sample was reduced and reacted in an elevated-pressure cell that was combined with the surface analysis system. The charge effect was calibrated by the C 1 s feature of the adventitious carbon (284.8 eV). The ultraviolet-visible (UV–vis) spectra were measured on a UV-2600 spectrophotometer (Shimadzu Co., Japan). N_2O titration was carried out on a Micromeritics Autochem II 2920 analyzer to determine the number of surface Cu° sites. The catalyst was first reduced in a H_2 flow at 250 °C for 2 h and then cooled down to 50 °C in a He flow. After a purge for 1 h, the He flow was switched into a flow of 1.0% N_2O/He gases. The produced N_2 was monitored with a thermal conductivity detector, which was used to calculate the number of surface Cu° sites according to the reaction of $2Cu(s) + N_2O(g) \rightarrow Cu_2O(s) + N_2(g)$ [37,38]. The transient absorption spectra were acquired using the pump and probe method with an amplified Ti:Sapphire femtosecond laser (Spitfire Ace-Spectra Physics, 35 fs (pulse width), 1 kHz (repetition rate), 5000 nm (central output wavelength)).

2.4. Catalyst test

Methanol synthesis reaction was carried out over 20 mg of catalyst (120–200 mesh) in a homemade fixed bed reactor (Fig. S1) under ambient pressure. The reaction temperature was 220 °C unless otherwise specified, which was precisely controlled by a TC-1000 controller (JASCO Corp.) with a thermocouple underneath the catalyst bed. Prior to reaction, the catalyst was reduced *in situ* in 20 ml min^{-1} H_2 at 250 °C for 2 h. After the reactor was cooled down to reaction temperature, the reactant gases consisting of 5 ml min^{-1} CO_2 and 15 ml min^{-1} H_2 were introduced. The effluent gases were analyzed with a Shimadzu GC-2014 gas chromatograph. Only methanol and CO were detected as products. The activity of the catalyst was described with methanol production rate (μmol methanol produced per gram of catalyst per min) and the data were collected after 0.5 h duration of reaction. For the photo-thermal catalysis, a LA-251Xe lamp (Hayashi) equipped with L42 + HA30 filters was employed as the visible light source (0.58 W cm^{-2}, $420 < \lambda < 800$ nm). The spectrum of the light source analyzed by a USR-40 spectrophotometer was shown in Fig. S2. $^{13}CO_2$ (Tokyo Gas Chemicals Co. Ltd.) was used instead of $^{12}CO_2$ in the isotopic labelling experiments.

2.5. In situ diffuse reflectance infrared Fourier transform spectroscopy (DRIFTS) studies

In situ DRIFTS studies were performed on an FT/IR-6300 spectrometer (JASCO Corp.) equipped with a diffuse reflectance attachment and with a liquid nitrogen-cooled mercury cadmium telluride (MCT) detector. 20 mg of catalyst powder was packed in a cell resembling the reactor used in catalyst testing experiments. The catalyst was reduced *in situ* in 20 ml min^{-1} H_2 at 250 °C for 2 h and then purged with 20 ml min^{-1} Ar at 250 °C for 1 h. After the catalyst was cooled down to 220 °C, a background spectrum was acquired in an Ar flow. Subsequently, the sample was exposed to the reactant gases consisting

of 5 ml min^{-1} CO_2 and 15 ml min^{-1} H_2. The spectra under dark and light conditions were recorded after 0.5 h under dark condition and after another 0.5 h under light condition respectively. The spectra were collected with 64 scans at a resolution of 4 cm^{-1}.

2.6. Electromagnetic field simulation

The electromagnetic fields distributed over the Cu/ZnO catalyst were simulated by the finite difference time domain (FDTD) method (FullWAVE, Synopsys' RSoft). The dielectric functions of Cu and ZnO were taken from [39] and [40] respectively. The simulation model used was shown in Fig. S3. The electromagnetic field propagated along the Z axis and oscillated along the X axis. The spatial distribution of the electromagnetic fields over the Cu/ZnO catalyst was stimulated at the peak wavelength of the surface plasmon resonance (~580 nm). The amplitude of the excited fields was normalized to 1.

3. Results and discussion

3.1. Catalyst characterization

The physico-chemical properties of the reduced Cu/ZnO catalyst with Cu/Zn molar ratio of 1/2 were characterized. As shown in Fig. 1a, N_2 sorption isotherms belonging to type IV were observed, indicating mesoporous characteristics of the Cu/ZnO catalyst. The specific surface area of 49.9 $m^2 g^{-1}$ is consistent with that in the literature [41]. XRD patterns in Fig. 1b indicated that metallic Cu and hexagonal wurtzite ZnO phases formed in the reduced catalyst. Based on Scherrer equation, the average crystallite size of Cu and ZnO was estimated as 14.3 and 17.9 nm respectively. The morphology of the catalyst was characterized with TEM. Fig. S4 depicts the peculiar microstructure of the Cu/ZnO catalyst, in which Cu and ZnO nanoparticles can hardly be distinguished from each other due to similar contrast [35,36]. By measuring the distance between lattice fringes in HR-TEM images (Fig. S4b), Cu and ZnO nanoparticles were identified. As shown in Fig. 1c, abundant Cu-ZnO interfaces were observed, which arerecognized as the active sites for methanol synthesis [42,43]. The average particle size of Cu and ZnO calculated from more than 100 nanoparticles was 15.2 and 18.4 nm respectively, in good agreement with that estimated from XRD patterns. The chemical state of the catalyst was characterized by XPS. As shown in Fig. S5a, metallic Cu with a Cu $2p_{3/2}$ peak at 932.1 eV was detected. The Zn $2p_{3/2}$ peak at 1021.7 eV corresponded to Zn^{2+} in ZnO (Fig. S5b) [9]. Because Cu $2p_{3/2}$ peaks of Cu° and Cu^+ have close position in binding energy [44,45], AES measurements were further carried out. As displayed in Fig. 1d, a broad peak with a maximum kinetic energy at 918.8 eV clearly indicates that metallic Cu° existed in the reduced Cu/ZnO catalyst [36,46]. The modified Auger parameter (α_{Cu} = BE(Cu $2p_{3/2}$) + KE(Cu_{LMM})) was 1850.9 eV, which was consistent with that of Cu° as well [44,47]. Cu species played crucial roles in methanol synthesis as the active sites for the dissociation of hydrogen and stabilization of the reaction intermediates [38]. Recent *in situ* XPS characterizations documented that metallic Cu was the active oxidation state of Cu in methanol synthesis [47]. All of the above physicochemical properties demonstrate that a prototype Cu/ZnO catalyst for methanol

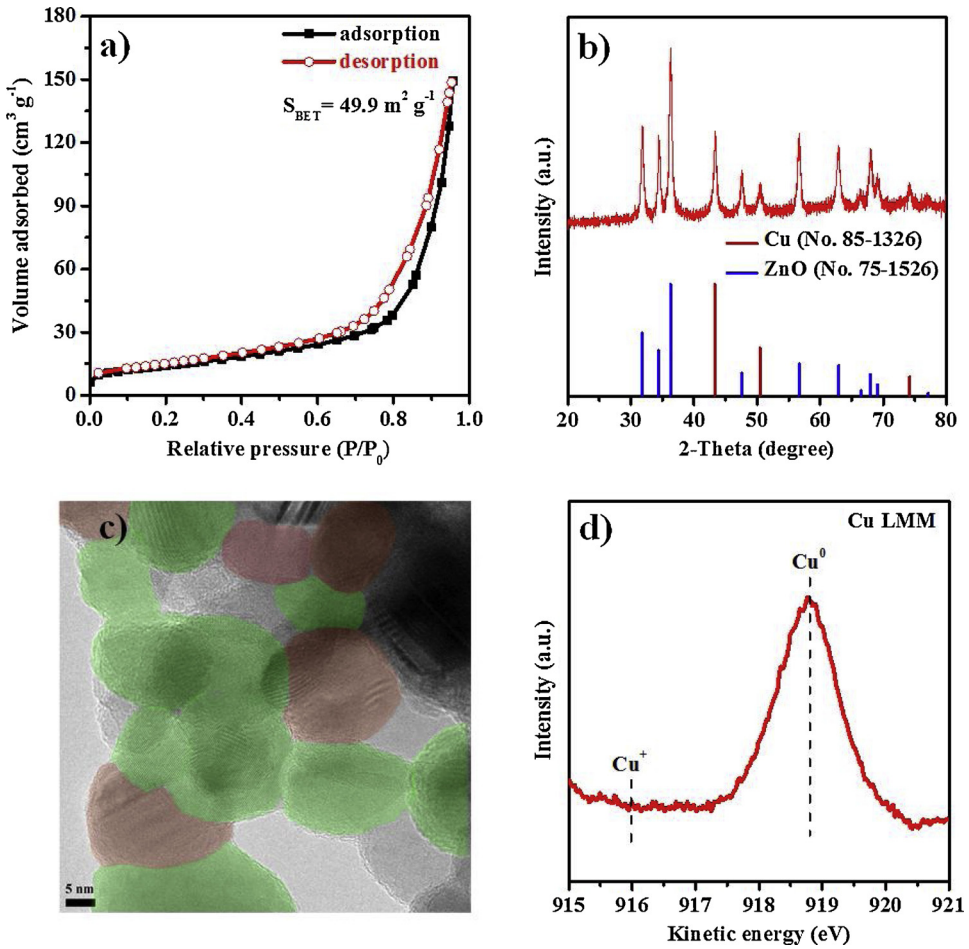

Fig. 1. Physicochemical characterizations of the reduced Cu/ZnO catalyst. (a) N_2 sorption isotherms; (b) XRD patterns; (c) HR-TEM image with Cu° in reddish brown and ZnO in light green; (d) Cu LMM AES spectrum. (For interpretation of the references to colour in this figure legend, the reader is referred to the web version of this article).

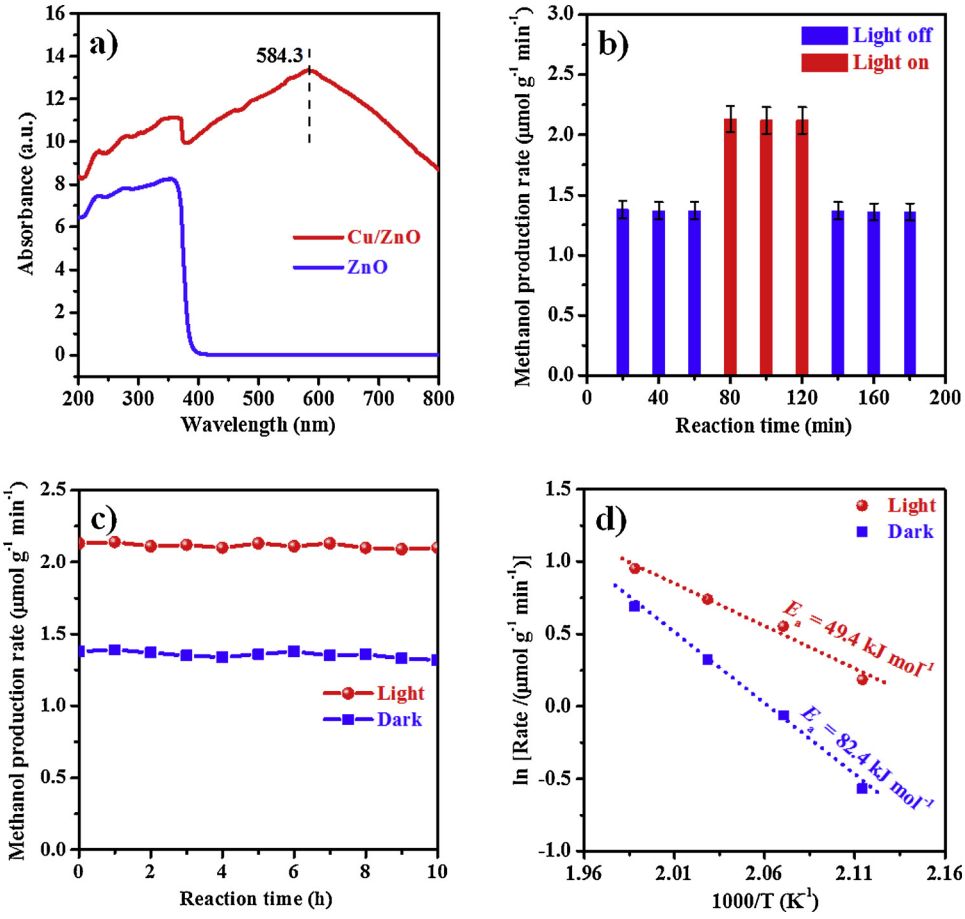

Fig. 2. Photo-promoted methanol synthesis over the Cu/ZnO catalyst under ambient pressure. (a) UV–vis absorption spectra of the Cu/ZnO catalyst and ZnO support; (b) Methanol production rate at 220 °C with and without visible light irradiation; (c) Stability tests at 220 °C under dark and light conditions; (d) Arrhenius plots under dark and light conditions.

synthesis has been synthesized.

3.2. Photo-enhanced methanol synthesis

Prior to investigate the catalytic activity of the Cu/ZnO catalyst in photo-thermal methanol synthesis, the optical properties of the samples were studied. Displayed in Fig. 2a are UV–vis absorption spectra of Cu/ZnO catalyst and ZnO support. A distinct absorption peak at 584.3 nm was observed on the Cu/ZnO catalyst, corresponding to the LSPR absorption of Cu nanoparticles in the visible range [10,48]. It was noted that LSPR peak of Cu nanoparticles was relatively broad, which might be caused by the slight surface oxidation as well as inhomogeneous distribution of size and shape [49–51]. Accordingly, a visible light source (0.58 W cm^{-2}, 420 < λ < 800 nm, Fig. S2) was introduced as the stimulus in the photo-thermal reaction that was carried out over the Cu/ZnO catalyst under ambient pressure. Fig. 2b shows that the catalytic activity was effectively promoted upon visible light irradiation and the light-induced promotion was fully reversible. Methanol production rate of the photo-thermal process (light on, 2.13 μmol g^{-1} min^{-1}) was 1.54 times as much as that of the pure thermal process (light off, 1.38 μmol g^{-1} min^{-1}). Notably, the enhancement in methanol yields by the photo-thermal strategy was much more significant than that achieved by the reported novel catalysts. Compared with the conventional Cu/ZnO catalyst in thermal catalysis, the methanol synthesis activity at 220 °C was promoted by 54% in the present work while less than 20% enhancement was realized over the Ni-Ga catalyst, a benchmark methanol synthesis catalyst under ambient pressure [19]. Based on the number of surface Cu° sites determined by N_2O titration, turnover frequency (TOF, methanol molecules produced per surface Cu atom per second) of the catalyst under dark and light condition was calculated as 5.9×10^{-5} and 9.1×10^{-5} s^{-1} respectively. Most of the methanol synthesis reactions in the literature were performed under elevated pressure, which makes the direct comparison of the TOF values over Cu/ZnO catalysts difficult [9,38]. However, we noticed that the TOF of the Cu/ZnO catalyst without light irradiation in this work was close with that of the $Cu/ZnO/Al_2O_3$ catalyst that was also tested at 220 °C under ambient pressure (5.1×10^{-5} s^{-1}, converted from Fig. 3 in [19]). Only methanol and CO were produced under the current reaction conditions. Similar promotion effect was observed on CO (Fig. S6). It is noteworthy to mention that CO was the major product under current reaction condition. As a matter of fact, it is the case that methanol is the minor product (with selectivity much lower than 50%) over most of the reported catalysts in low-pressure methanol synthesis [19–21,52]. Considering that methanol is much more valuable than CO, the major topic in the present work is about methanol synthesis. Fig. 2c demonstrates that the catalyst was relatively stable under both dark and light conditions. CO_2 conversion and methanol selectivity as a function of time under dark and light conditions were displayed in Fig. S7. The low CO_2 conversion demonstrates that the catalysts were run in the differential regime, far from equilibrium [21,52]. The chemical state of Cu species after stability test under dark condition was characterized by XPS (Fig. S8a) and AES (Fig. S8b). By comparing XPS and AES spectra between before and after reaction, it was confirmed that metallic Cu was stable during reaction, consistent with the steady catalytic performance observed. Fig. 2d presents the Arrhenius plots of the Cu/ZnO catalyst under dark and light conditions. It is noted that the apparent activation energy (E_a) was reduced by 40% from 82.4 to 49.4 kJ mol^{-1} upon visible light irradiation. This phenomenon has been reported previously, which indicates that the hot electrons excited by LSPR on Cu nanoparticles assisted the activation of reaction intermediates during methanol synthesis [33,53]. Control experiments (Fig. S9) substantiate that both external and internal diffusion have been eliminated

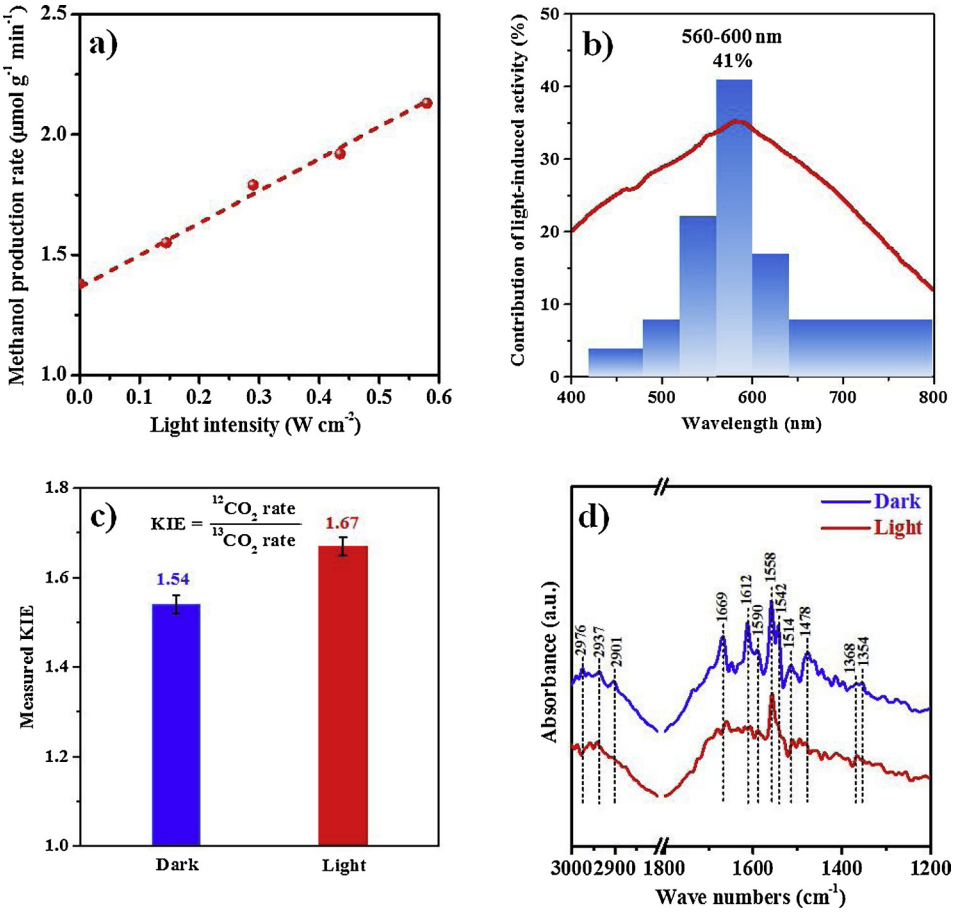

Fig. 3. The role of light on methanol synthesis over the Cu/ZnO catalyst. (a) Dependence of activity on light intensity; (b) Dependence of activity on light wavelength (the contribution of light-induced activity was described by the percentage of the activity enhancement induced by light in the specific wavelength range out of that induced by light in the whole visible range); (c) Influence of visible light on *KIE*; (d) *In situ* DRIFTS spectra under dark and light conditions.

over the Cu/ZnO catalyst under light condition [54].

To unravel the role of light on methanol synthesis, the dependence of activity on light intensity and wavelength was investigated. Fig. 3a shows a linear increase in activity as a function of light intensity, suggesting a hot electron driven catalysis in photo-thermal reaction [55]. The dependence of activity on light wavelength was established using various optical filters with similar light intensity among various wavelength ranges (Table S1). The close correlation between the contribution of light-induced activity and the optical absorption caused by LSPR on Cu nanoparticles further manifests that surface plasmons are responsible for the promoted activity (Fig. 3b) [28–33]. Another distinct signature for the electron driven catalysis is the enhanced kinetic isotope effect (*KIE*) ($^{12}CO_2$ rate/$^{13}CO_2$ rate) under light condition, which was substantiated in the present work as well (Fig. 3c) [29,55]. All of the above experimental signatures conclusively demonstrate that the hot electrons excited by LSPR on Cu nanoparticles play a crucial role in promoting the methanol production rate. In addition, the impact of hot electrons on the reaction intermediates was studied by *in situ* DRIFTS spectra. According to the literature [21,40,56], the bands shown in Fig. 3d are assigned as *HCOO (formate) species on ZnO (2976, 1590, 1558 and 1368 cm^{-1}), *HCOO species on Cu (2901, 1669, 1542 and 1354 cm^{-1}), *CH_3O (methoxy) species on ZnO (2937 cm^{-1}), and other carbon containing species on the surface (1612, 1514 and 1478 cm^{-1}), which points to a formate pathway in methanol synthesis [42,43]. Comparatively, the intensity of the reaction intermediates was substantially attenuated after the light was turned on, suggesting more facile activation of the adsorbed intermediates with the aid of photo-excited hot electrons [9,33]. Recent studies based on density functional theory (DFT) calculations demonstrated that the energetic charge carriers (electron/hole pairs) from the plasmonic nanoparticles would facilitate the activation of the adsorbed intermediates by attaching themselves to the adsorbates on the surface of excited catalysts, leading to enhanced catalytic activity under light irradiation [25,33].

To understand the mechanism of the visible light promoted methanol synthesis, the plasmon excitation over the Cu/ZnO catalyst was stimulated by the finite difference time domain (FDTD) method (see Fig. S3 for the simulation model). Fig. 4a displays the simulated electromagnetic field distributions of the Cu/ZnO catalyst under light irradiation at the peak wavelength of the surface plasmon resonance (580 nm). Enhanced electric fields were clearly noticed on the surface of plasmonic Cu nanoparticles, which would excite abundant hot electrons. In addition, the electron transfer dynamics at Cu-ZnO interfaces was characterized by femtosecond (fs) transient absorption spectra. A Cu/ZrO_2 catalyst was employed as the reference to examine the response from excited Cu nanoparticles because electron transfer from Cu to ZrO_2 would not occur due to the high conduction band of ZrO_2 [57,58]. As shown in Fig. 4b, no transient absorption was detected over the Cu/ZrO_2 catalyst, suggesting that excited Cu nanoparticles would not induce any transient absorption. In contrast, a distinct transient absorption was observed over the Cu/ZnO catalyst, which would be induced by electrons injected to conduction band of ZnO [59,60]. Therefore, transient absorption kinetics studies demonstrate that hot electrons would be effectively transferred from Cu nanoparticles to ZnO support. It is well known that Cu-ZnO interfaces play a vital role in CO_2 hydrogenation into methanol [42,43]. Nevertheless, the exact mechanism how ZnO influences the methanol synthesis over Cu catalysts is still under debate. Generally, two hypotheses were proposed. One acknowledged ZnO as a structural modifier or promoter for intermediate activation, leading to an enhanced activity on Cu active sites by the unique Cu-ZnO synergy [9,61,62]. The other one suggested the decoration of Cu surface with partially reduced ZnO_x or metallic Zn, creating the very active ensembles for methanol production

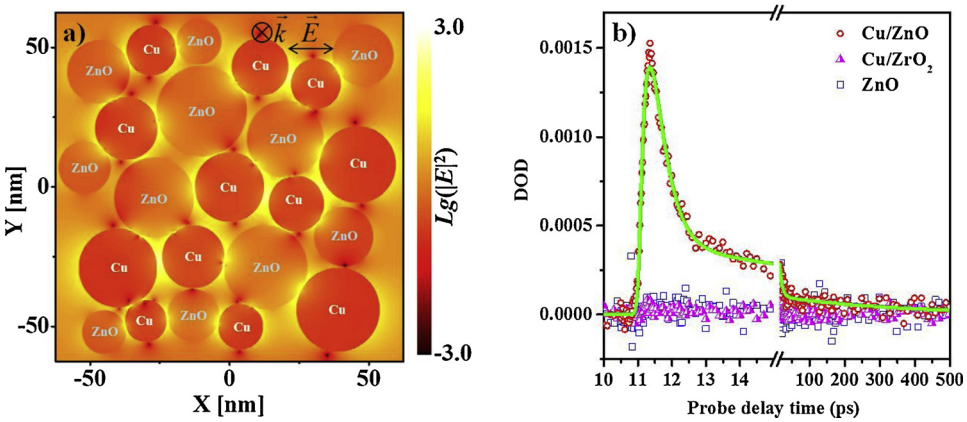

Fig. 4. (a) Spatial distribution of the electromagnetic fields over the Cu/ZnO catalyst under 580 nm irradiation stimulated using the FDTD method; (b) Transient absorption kinetics studies over the Cu/ZnO catalyst under photo-excitation at 580 nm, in which the electron transfer was accomplished within 502 fs corresponding to the distinct rise in the spectrum. Cu/ZrO_2 and ZnO samples were employed as references in transient absorption kinetics studies, in which no transient absorption rise was observed.

[63,64]. In both cases, the facile photo-induced electron transfer through Cu-ZnO interfaces would facilitate the activation of the adsorbates adjacent to the metal-support interfaces.

3.3. General discussion

Based on the experimental signatures (Fig. 3) and theoretical studies (Fig. 4), a mechanism combining the photo-exited hot electrons on the Cu nanoparticles and the electron transfer through the metal-support interfaces was proposed to rationalize the visible light promoted methanol synthesis (Fig. 5). In the pure thermal process, methanol synthesis proceeded along a formate pathway through *HCOO, *HCOOH, $*H_2COOH$ and $*CH_3O$ intermediates, among which only *HCOO and $*CH_3O$ species were observed in *in situ* DRIFT spectra due to their strong adsorption [42,43]. Based on DFT calculations in the literature [9,42,43], the hydrogenation of *HCOOH was generally acknowledged as the rate-limiting step. In the photo-thermal process, a similar reaction pathway occurred based on the *in situ* DRIFTS spectra (Fig. 3d). However, the photo-excited hot electrons on the Cu nanoparticles and adjacent to the Cu-ZnO interfaces would be scattered into the adsorbed reaction intermediates, weakening the chemical bonds [29,33]. In the meantime, the hot holes remained on Cu surfaces, which would be combined with the back-transferred hot electrons [25,29,65,66]. The facilitated activation of *HCOO species corresponding to the attenuated *in situ* DRIFT intensity upon light irradiation would alleviate the surface poisoning of the Cu/ZnO catalyst caused by the accumulation of *HCOO species [9,43]. Consequently, the methanol production rate was enhanced under visible light irradiation. Notably, little change was observed towards methanol selectivity with the introduction of visible light. It should be clarified that the reduced activation energy does not necessarily alter the product selectivity. Instead, the catalytic reaction under light illumination may still proceed with a similar reaction pathway but at a faster rate [33,67,68].

In addition, the visible light promoted methanol synthesis was observed on Cu/ZnO catalysts with various Cu/Zn molar ratios (Figs. S10 and S11). We also investigated methanol synthesis over Cu catalysts supported on other oxides, in which the visible light promoted methanol synthesis was confirmed over the Cu/CeO_2 catalyst although much lower activity was detected (Figs. S12 and S13). Negligible methanol was detected over Cu/TiO_2 and Cu/ZrO_2 catalyst under the present reaction condition (220 °C and 1 atm). The above results manifest the crucial role of ZnO support in Cu-based catalysts for methanol synthesis [11,41].

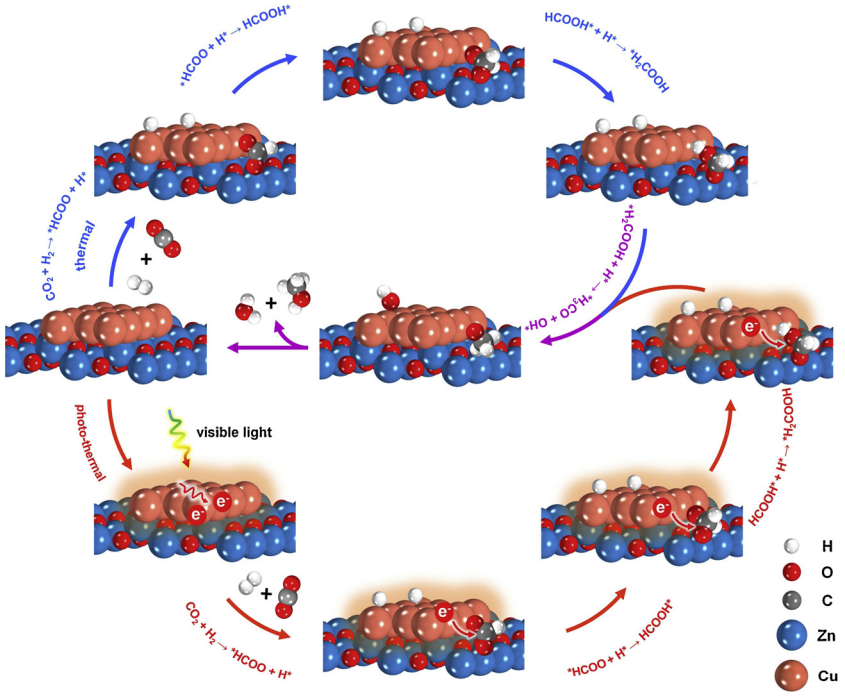

Fig. 5. A mechanism proposed for the visible light promoted methanol synthesis. The photo-thermal methanol synthesis follows a similar formate pathway as the pure thermal methanol synthesis, which proceeds along *HCOO, *HCOOH, $*H_2COOH$ and $*CH_3O$ intermediates with the hydrogenation of *HCOOH as the rate-limiting step. The photo-excited hot electrons on the Cu nanoparticles and adjacent to the Cu-ZnO interfaces synergistically promote the activation of reaction intermediates, which lowers the reaction barrier and enhances the methanol production rate.

4. Conclusions

In conclusion, visible light promoted methanol synthesis over plasmonic Cu/ZnO catalysts under ambient pressure was reported for the first time. Upon visible light irradiation, the methanol production rate increased from 1.38 to 2.13 $\mu mol\, g^{-1}\, min^{-1}$ and the apparent activation energy decreased from 82.4 to 49.4 $kJ\, mol^{-1}$. Based on experimental signatures and theoretical studies, a mechanism combining the photo-exited hot electrons on the Cu nanoparticles and electron transfer through the metal-support interfaces was proposed. The hot electrons on Cu and ZnO synergistically facilitated the activation of reaction intermediates, leading to photo-promoted methanol synthesis. This work opens up a new route to promote liquid fuel synthesis from CO_2 reduction and provides new insights into photochemical transformations on plasmonic nanostructures.

Acknowledgements

This work was financially supported by JSPS KAKENHI (No. JP18H02065), the World Premier International Research Center Initiative (WPI Initiative) on Materials Nanoarchitectonics (MANA), MEXT (Japan), National Basic Research Program of China (973 Program, No. 2014CB239301), National Natural Science Foundation of China (No. 21633004, No. 21776007, No. 21811530293), Scholarship by China Scholarship Council (CSC) (No. 201606320239, No. 201706885023), and the Fundamental Research Funds for the Central Universities (XK1802-1).

Appendix A. Supplementary data

Supplementary material related to this article can be found, in the online version, at doi:https://doi.org/10.1016/j.apcatb.2019.03.003.

References

[1] E. Pipelzadeh, V. Rudolph, G. Hanson, C. Noble, L. Wang, Appl. Catal. B 218 (2017) 672–678.
[2] J. Qin, S. Wang, X. Wang, Appl. Catal. B 209 (2017) 476–482.
[3] H. Liu, T.D. Dao, L. Liu, X. Meng, T. Nagao, J. Ye, Appl. Catal. B 209 (2017) 183–189.
[4] G. Liu, X. Meng, H. Zhang, G. Zhao, H. Pang, T. Wang, P. Li, T. Kako, J. Ye, Angew. Chem. Int. Ed. 56 (2017) 5570–5574.
[5] F. Pan, W. Deng, C. Justiniano, Y. Li, Appl. Catal. B 226 (2018) 463–472.
[6] K.K. Ghuman, L.B. Hoch, P. Szymanski, J.Y.Y. Loh, N.P. Kherani, M.A. El-Sayed, G.A. Ozin, C.V. Singh, J. Am. Chem. Soc. 138 (2016) 1206–1214.
[7] S. Kattel, B. Yan, J.G. Chen, P. Liu, J. Catal. 343 (2016) 115–126.
[8] J. Ye, C. Liu, D. Mei, Q. Ge, ACS Catal. 3 (2013) 1296–1306.
[9] S. Kattel, P.J. Ramírez, J.G. Chen, J.A. Rodriguez, P. Liu, Science 355 (2017) 1296–1299.
[10] B. An, J. Zhang, K. Cheng, P. Ji, C. Wang, W. Lin, J. Am. Chem. Soc. 139 (2017) 3834–3840.
[11] W. Wang, S. Wang, X. Ma, J. Gong, Chem. Soc. Rev. 40 (2011) 3703–3727.
[12] IHS, Technical Report for IHS Chemical, IHS Chemical, Englewood, 2016, p. 1.
[13] N. Rui, Z. Wang, K. Sun, J. Ye, Q. Ge, C.-j. Liu, Appl. Catal. B 218 (2017) 488–497.
[14] M. Aresta, A. Dibenedetto, Dalton Trans. (2007) 2975–2992.
[15] O. Martin, A.J. Martín, C. Mondelli, S. Mitchell, T.F. Segawa, R. Hauert, C. Drouilly, D. Currulla-Ferré, J. Pérez-Ramírez, Angew. Chem. Int. Ed. 55 (2016) 6261–6265.
[16] J. Ye, Q. Ge, C.-j. Liu, Chem. Eng. Sci. 135 (2015) 193–201.
[17] S. Du, W. Tang, X. Lu, S. Wang, Y. Guo, P.-X. Gao, Adv. Mater. Interfaces (2017) 1700730.
[18] C. Liu, B. Yang, E. Tyo, S. Seifert, J. DeBartolo, B. von Issendorff, P. Zapol, S. Vajda, L.A. Curtiss, J. Am. Chem. Soc. 137 (2015) 8676–8679.
[19] F. Studt, I. Sharafutdinov, F. Abild-Pedersen, C.F. Elkjær, J.S. Hummelshøj, S. Dahl, I. Chorkndoff, J.K. Nørskov, Nat. Chem. 6 (2014) 320–324.
[20] X. Yang, S. Kattel, S.D. Senanayake, J.A. Boscoboinik, X. Nie, J. Graciani, J.A. Rodriguez, P. Liu, D.J. Stacchiola, J.G. Chen, J. Am. Chem. Soc. 137 (2015) 10104–10107.
[21] A.R. Richard, M. Fan, ACS Catal. 7 (2017) 5679–5692.
[22] J. Ding, Z. Dai, F. Qin, H. Zhao, S. Zhao, R. Chen, Appl. Catal. B 205 (2017) 281–291.
[23] J. Ding, Z. Dai, F. Tian, B. Zhou, B. Zhao, H. Zhao, Z. Chen, Y. Liu, R. Chen, J. Mater. Chem. A 5 (2017) 23453–23459.
[24] X. Meng, L. Liu, S. Ouyang, H. Xu, D. Wang, N. Zhao, J. Ye, Adv. Mater. 28 (2016) 6781–6803.
[25] S. Linic, U. Aslam, C. Boerigter, M. Morabito, Nat. Mater. 14 (2015) 567–576.
[26] X. Chang, T. Wang, J. Gong, Energy Environ. Sci. 9 (2016) 2177–2196.
[27] Z. Yin, Y. Wang, C. Song, L. Zheng, N. Ma, X. Liu, S. Li, L. Lin, M. Li, Y. Xu, W. Li, G. Hu, Z. Fang, D. Ma, J. Am. Chem. Soc. 140 (2018) 864–867.
[28] C.-H. Hao, X.-N. Guo, Y.-T. Pan, S. Chen, Z.-F. Jiao, H. Yang, X.-Y. Guo, J. Am. Chem. Soc. 138 (2016) 9361–9364.
[29] P. Christopher, H. Xin, S. Linic, Nat. Chem. 3 (2011) 467–472.
[30] L.-M. Lyu, Y.-C. Kao, D.A. Cullen, B.T. Sneed, Y.-C. Chuang, C.-H. Kuo, Chem. Mater. 29 (2017) 5681–5692.
[31] H. Liu, X. Meng, T.D. Dao, H. Zhang, P. Li, K. Chang, T. Wang, M. Li, T. Nagao, J. Ye, Angew. Chem. Int. Ed. 54 (2015) 11545–11549.
[32] H. Liu, M. Li, T.D. Dao, Y. Liu, W. Zhou, L. Liu, X. Meng, T. Nagao, J. Ye, Nano Energy 26 (2016) 398–404.
[33] H. Song, X. Meng, T.D. Dao, W. Zhou, H. Liu, L. Shi, H. Zhang, T. Nagao, T. Kako, J. Ye, ACS Appl. Mater. Interfaces 10 (2018) 408–416.
[34] H.V. Thang, S. Tosoni, G. Pacchioni, ACS Catal. 8 (2018) 4110–4119.
[35] M. Behrens, R. Schlögl, Z. Anorg. Allg. Chem. 639 (2013) 2683–2695.
[36] X. Yang, H. Chen, Q. Meng, H. Zheng, Catal. Sci. Technol. 7 (2017) 5625–5634.
[37] G.C. Chinchen, C.M. Hay, H.D. Vandervell, K.C. Waugh, J. Catal. 103 (1987) 79–86.
[38] B. Rungtaweevoranit, J. Baek, J.R. Araujo, B.S. Archanjo, K.M. Choi, O.M. Yaghi, G.A. Somorjai, Nano Lett. 16 (2016) 7645–7649.
[39] A.D. Rakić, A.B. Djurišić, J.M. Elazar, M.L. Majewski, Appl. Opt. 37 (1998) 5271–5283.
[40] T.D. Dao, S. Ishii, T. Yokoyama, T. Sawada, R.P. Sugavaneshwar, K. Chen, Y. Wada, T. Nabatame, T. Nagao, ACS Photonics 3 (2016) 1271–1278.
[41] R. Fan, M. Kyodo, L. Tan, X. Peng, G. Yang, Y. Yoneyama, R. Yang, Q. Zhang, N. Tsubaki, Fuel. Process. Technol. 167 (2017) 69–77.
[42] K. Larmier, W.-C. Liao, S. Tada, E. Lam, R. Verel, A. Bansode, A. Urakawa, A. Comas-Vives, C. Copéret, Angew. Chem. Int. Ed. 56 (2017) 2318–2323.
[43] S. Kattel, P. Liu, J.G. Chen, J. Am. Chem. Soc. 139 (2017) 9739–9754.
[44] C.D. Wagner, W.M. Riggs, L.E. Davis, J.F. Moulder, G.E. Mullenberg, Handbook of X-ray Photoelectron Spectroscopy, Perkin-Elmer, MN, 1979.
[45] J.H. Lee, S.W. Kim, B.S. Ahn, D.J. Moon, J. Nanosci. Nanotechnol. 15 (2015) 400–403.
[46] R. Zhang, P. Li, R. Xiao, N. Liu, B. Chen, Appl. Catal. B 196 (2016) 142–154.
[47] S. Natesakhawat, J.W. Lekse, J.P. Baltrus, P.R. Ohodnicki Jr., B.H. Howard, X. Deng, C. Matranga, ACS Catal. 2 (2012) 1667–1676.
[48] S.D. Pike, A. García-Trenco, E.R. White, A.H.M. Leung, J. Weiner, M.S.P. Shaffer, C.K. Williams, Catal. Sci. Technol. 7 (2017) 3842–3850.
[49] Y. Bu, S. Er, J.W.H. Niemantsverdriet, H.O.A. Fredriksson, J. Catal. 357 (2018) 176–187.
[50] Z. Wei, L. Rosa, K. Wang, M. Endo, S. Juodkazis, B. Ohtani, E. Kowalska, Appl. Catal. B 206 (2017) 393–405.
[51] Z. Wei, M. Janczarek, M. Endo, C. Colbeau-Justin, B. Ohtani, E. Kowalska, Catal. Today 310 (2018) 19–25.
[52] J. Díez-Ramírez, F. Dorado, A.R. de la Osa, J.L. Valverde, P. Sánchez, Ind. Eng. Chem. Res. 56 (2017) 1979–1987.
[53] X. Zhang, X. Li, D. Zhang, N.Q. Su, W. Yang, H.O. Everitt, J. Liu, Nat. Commun. 8 (2017) 14542.
[54] C. Wang, P. Zhai, Z. Zhang, Y. Zhou, J. Zhang, H. Zhang, Z. Shi, R.P.S. Han, F. Huang, D. Ma, J. Catal. 334 (2016) 42–51.
[55] S. Linic, P. Christopher, D.B. Ingram, Nat. Mater. 10 (2011) 911–921.
[56] R. Yang, Y. Fu, Y. Zhang, N. Tsubaki, J. Catal. 228 (2004) 23–35.
[57] A. Furube, L. Du, K. Hara, R. Katoh, M. Tachiya, J. Am. Chem. Soc. 129 (2007) 14852–14853.
[58] H. Song, X. Meng, Z.-j. Wang, Z. Wang, H. Chen, Y. Weng, F. Ichihara, M. Oshikiri, T. Kako, J. Ye, ACS Catal. 8 (2018) 7556–7565.
[59] Y. Tian, T. Tatsuma, J. Am. Chem. Soc. 127 (2005) 7632–7637.
[60] Y. Nishijima, K. Ueno, Y. Yokota, K. Murakoshi, H. Misawa, J. Phys. Chem. Lett. 1 (2010) 2031–2036.
[61] S.A. Kondrat, P.J. Smith, P.P. Wells, P.A. Chater, J.H. Carter, D.J. Morgan, E.M. Fiordaliso, J.B. Wagner, T.E. Davies, L. Lu, J.K. Bartley, S.H. Taylor, M.S. Spencer, C.J. Kiely, G.J. Kelly, C.W. Park, M.J. Rosseinsky, G.J. Hutchings, Nature 531 (2016) 83–87.
[62] O. Martin, C. Mondelli, A. Cervellino, D. Ferri, D. Curulla-Ferré, J. Pérez-Ramírez, Angew. Chem. Int. Ed. 55 (2016) 11031–11036.
[63] M. Behrens, F. Studt, I. Kasatkin, S. Kühl, M. Hävecker, F. Abild-Pedersen, S. Zander, F. Girgsdies, P. Kurr, B.-L. Kniep, M. Tovar, R.W. Fischer, J.K. Nørskov, R. Schlögl, Science 336 (2012) 893–897.
[64] M. Behrens, S. Zander, P. Kurr, N. Jacobsen, J. Senker, G. Koch, T. Ressler, R.W. Fischer, R. Schlögl, J. Am. Chem. Soc. 135 (2013) 6061–6068.
[65] P. Christopher, H. Xin, A. Marimuthu, S. Linic, Nat. Mater. 11 (2012) 1044–1050.
[66] H. Li, F. Qin, Z. Yang, X. Cui, J. Wang, L. Zhang, J. Am. Chem. Soc. 139 (2017) 3513–3521.
[67] K.K. Ghuman, L.B. Hoch, P. Szymanski, J.Y.Y. Loh, N.P. Kherani, M.A. El-Sayed, G.A. Ozin, C.V. Singh, J. Am. Chem. Soc. 138 (2016) 1206–1214.
[68] M. Ghoussoub, M. Xia, P.N. Duchesne, D. Segal, G. Ozin, Energy Environ. Sci. (2019), https://doi.org/10.1039/c8ee02790k in press.